High thermopower and potential thermoelectric properties of crystalline LiH and NaH

Yinchang Zhao,[1,*] Zhenhong Dai,[1,†] Chao Zhang,[1] Chao Lian,[2] Shuming Zeng,[3,4] Geng Li,[3,4] Sheng Meng,[2,4,‡] and Jun Ni[3,4,§]

[1]*Department of Physics, Yantai University, Yantai 264005, People's Republic of China*

[2]*Beijing National Laboratory for Condensed Matter Physics and Institute of Physics, Chinese Academy of Sciences, Beijing, 100190, People's Republic of China*

[3]*State Key Laboratory of Low-Dimensional Quantum Physics, Department of Physics, Tsinghua University, Beijing 100084, People's Republic of China*

[4]*Collaborative Innovation Center of Quantum Matter, Beijing 100084, People's Republic of China*

(Received 21 September 2016; revised manuscript received 26 November 2016; published 23 January 2017)

We use first-principles calculations combined with the Boltzmann transport equation and semiclassical analysis to investigate the thermal conductivity κ, electrical conductivity σ, and thermopower S of crystalline LiH and NaH. Remarkably, the calculated S is extraordinarily high while the lattice thermal conductivity κ_L is fairly low, which, as a result, leads to a much high thermoelectric power factor σS^2 and good thermoelectric properties, with the figure of merit zT even larger than 1.5 in the p-type doped NaH. Further analyses reveal that (i) the large band gap and the flat band around the Fermi level cause the high S and (ii) strong anharmonic phonon scatterings and relevant phonon group velocities result in the low κ_L in these light materials. Our results support that crystalline LiH and NaH may be potential materials for thermoelectric applications.

DOI: 10.1103/PhysRevB.95.014307

I. INTRODUCTION

Thermoelectric (TE) materials have attracted great interests due to their power to convert heat into electricity, which offers a clean way to recover the waste heat from the high-temperature industrial or the transportation applications [1–4]. For a TE power generator, the conversion efficiency at temperature T is defined by the dimensionless figure of merit $zT = \sigma S^2 T/\kappa$, where σ is the electrical conductivity, S is the thermopower (also known as Seebeck coefficient), and κ is the thermal conductivity, which consists of the lattice thermal conductivity κ_L and the electronic contribution κ_{el}. Hence a complete picture to reveal TE properties requires investigating both the electronic and the thermal transport properties, while the power factor σS^2 is often used to estimate the TE features. In semiconductors, because κ_{el} is directly related to σ via the Wiedemann-Franz formula $\kappa_{el} = L\sigma T$ (L is the Lorenz number), optimization of the figure of merit zT always suffers from the interdependence between σ and κ_{el}, which implies there is almost no room to tune κ_{el} independently. Therefore, to increase zT, researchers have been turning to seek out solutions to enhance the power factor σS^2 or to reduce the lattice thermal conductivity κ_L [5–17].

There have been many strategies proposed for the enhancement of the power factor σS^2. For instance, due to a drastic improvement of S resulted from a distortion of the electronic density of states (EDOS) by the resonant impurities, a high zT of 1.5 was achieved at 773 K in the Tl-doped p-type PbTe [2,14]. The quantum confinement effect in low-dimensional Bi_2Te_3 caused the increase of zT by a factor of 13 over the bulk value since σ and S can be tuned by a highly anisotropic effective-mass tensor [15]. The maximum value of $zT \sim 1.3$ was obtained in $Mg_2 Si_{1-x} Sn_x$ solid solutions because of the conduction band convergence, which leads to a significantly enhanced S with no adverse effect on the carrier mobility [16]. In addition, σS^2 can be also increased by the electron energy filtering scheme that filters out the low-energy carriers from the transport through heterostructure barriers [18,19]. As an example, in solution-processed $Sb_2 Te_3$ with inserted Ag nanoparticles as nonplanar barriers, σS^2 and zT were enhanced drastically owing to the carrier energy filtering effect [20].

Besides these approaches to meliorating TE properties, the reductions of κ_L have caused significant enhancements of zT via increased phonon scattering around interfaces, structural defects, and grain boundaries in the nanostructured materials [21,22]. For example, because of the significant reduction of κ_L to about 0.5 W m^{-1} K^{-1} via all-scale hierarchical structures, a high zT of 2.2 was reported in the bulk spark-plasma-sintered Na-doped PbTe:SrTe at 900 K [23]; a zT of 2.0 was achieved in the Na-doped PbTe at 773 K through further optimization of nanostructures to reduce κ_L [24]. Recently, an extraordinary zT of 2.6 was reported in the undoped monocrystalline SnSe at 923 K with no nanostructuring or complex alloying but only the ultralow intrinsic κ_L of the crystal [25]. However, later researches reported that the zT of the doped polycrystalline SnSe is only 0.6–0.7 [26,27]. Also a theoretical study for SnSe indicated that the actual κ_L of the crystalline direction (b axis), along which the highest value of zT is achieved, could be higher than the κ_L reported in Ref. [25], which suggests a further research on the results [28]. In addition, there are a great many other materials with lower κ_L and good TE properties, such as CdO [11], $IrSb_3$ [29], $PbTiO_3$ [30], n-type TiO_2 polymorphs [31], fully filled skutterudite $YbFe_4 Sb_{12}$ [12], and nanoporous bulk silicon [13], etc. From the perspective of composition, all of these materials contain heavier atoms, which is beneficial for increasing the phonon scattering and thus helps to reduce κ_L.

Ideally, the materials with both high σS^2 and low κ will be the best candidates for TE applications. In this paper, we take the ultralight ionic crystal LiH and NaH as an example to

*y.zhao@ytu.edu.cn
†zhdai@ytu.edu.cn
‡smeng@iphy.ac.cn
§junni@mail.tsinghua.edu.cn

systematically investigate the thermal and electronic transport properties, and conclude that these materials have high thermopower S, low lattice thermal conductivity κ_L, and consequently good TE properties. Moreover, the findings for low κ_L of these light materials are in sharp contrast with previous results that materials with lower κ_L always possess heavier atomic masses. These results support that ionic crystal LiH and NaH are potential candidates for TE applications. Calculation details are described in Sec. II. The results on thermal and electronic transport properties are presented in Sec. III. Section IV is our summary.

II. METHODOLOGY

We study the thermal transport properties firstly. From the solution of Boltzmann transport equation (BTE) [32], the lattice thermal conductivity along the x direction is defined as

$$\kappa_{\mathrm{L}}^{xx} = \frac{1}{k_B T^2 \Omega N} \sum_{\lambda} f_0(f_0+1)(\hbar\omega_\lambda)^2 v_g^{x,\lambda} F_\lambda^x, \qquad (1)$$

where k_B, Ω, and N are the Boltzmann constant, the volume of the unit cell, and the number of q points in the first Brillouin zone, respectively. f_0 is the equilibrium Bose-Einstein distribution function. ω_λ is the phonon frequency at the phonon mode λ, which consists of both the wave vector q and the phonon branch ν. $\hbar$ is the reduced Planck constant, and $v_g^{x,\lambda}$ is the phonon group velocity of mode λ along the x direction. F_λ^x is given by [32]

$$F_\lambda^x = \tau_\lambda \left(v_g^{x,\lambda} + \Delta_\lambda\right), \qquad (2)$$

where τ_λ is the lifetime in phonon relaxation time approximation (RTA). Δ_λ is a correction term which eliminates the inaccuracy of RTA by solving the BTE iteratively. If Δ_λ is equal to zero, the RTA result for κ_{L}^{xx} is obtained.

The SHENGBTE code [32] is used to calculate κ_{L}. The harmonic and anharmonic interatomic force constants (IFCs) required in SHENGBTE calculations are computed based on the density functional theory (DFT) software package VASP [33,34] combined with the PHONOPY program [35] and the THIRDORDER.PY script supplied with SHENGBTE, respectively. The IFC2 is generated with $5 \times 5 \times 5$ supercells by the finite-difference approach in PHONOPY. The anharmonic IFC3 is obtained with $4 \times 4 \times 4$ supercells via the same finite-difference approach in THIRDORDER.PY, and interaction up to third nearest neighbors is included in these calculations. In DFT calculations, the ion cores are modeled by the projector augmented wave potentials (PAW) [36], the valance electrons are modeled by a plane-wave basis set with the cutoff energy of 520 eV and the exchange-correlation functional of generalized gradient approximation (GGA) of Perdew-Burke-Ernzerhof (PBE) [37]. For relaxation of the primitive cell, the force acting on each atom is less than 10^{-8} eV/Å with the electronic stopping criterion of 10^{-8} eV. A $15 \times 15 \times 15$ Γ-centered Monkhorst-Pack k-point mesh is utilized to simulate the Brillouin zone integration of the primitive cell, while only the Γ point is used for calculations of the supercells generated by the finite-difference approach. To estimate the dielectric tensor and Born effective charges required in both PHONOPY and SHENGBTE calculations, density functional perturbation theory (DFPT) coded in VASP is utilized with the k mesh of $45 \times 45 \times 45$. At last, for SHENGBTE calculations, a q mesh of $30 \times 30 \times 30$ is used to simulate the corresponding **q** space integration.

To calculate σ, S, and κ_{el}, the semiclassical Boltzmann theory and the rigid-band approach implemented in the BOLTZTRAP code [38] is utilized within the constant scattering time approximation. The electronic structure is recalculated by VASP on a dense k mesh of $60 \times 60 \times 60$ to obtain derivatives of the Kohn-Sham eigenvalues. The only empirical parameter in this approach is the scattering time τ, which determines the value of σ and κ_{el}. Experimental results on carrier concentration, mobility, and σ can be employed to estimate τ. Here, because of the lack of experimental data on conductive characters of LiH and NaH, the value of τ from 1 to 10 fs is used as a substitute.

III. RESULTS AND DISCUSSION

LiH and NaH are both rock-salt structures. Their optimized lattice constants are 4.00 and 4.83 Å, respectively, which are consistent with the experimental values of 4.08 and 4.89 Å [39–43]. The calculated phonon dispersion and phonon density of states (PDOS) of them are plotted in Fig. 1. There are six branches: two transverse acoustic (TA), one longitudinal acoustic (LA), two transverse optical (TO), and one longitudinal optical (LO) modes. The partial PDOS shows that almost all of the acoustic vibrations are afforded by the alkaline metal atoms, while most of the optical modes originate from the hydrogen atoms. The acoustic and optical branches

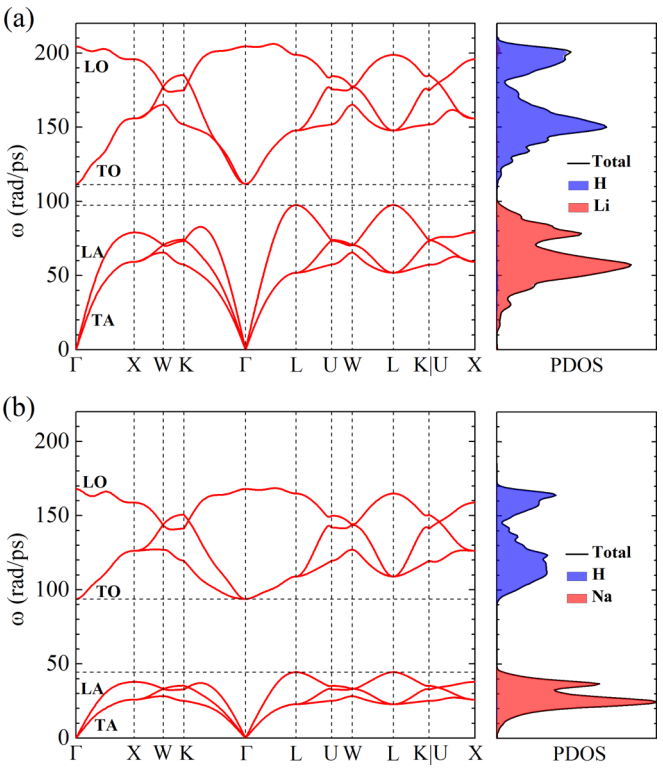

FIG. 1. Phonon dispersion and PDOS of LiH (a) and NaH (b). The acoustic (optical) branches arise almost completely from the vibrations of alkaline metal atoms (hydrogen atoms).

are separated by a gap of about 14.4 and 49.3 rad/ps for LiH and NaH, respectively. In polar semiconductors and ionic crystals, the optical modes always display the splitting of LO and TO around the Γ point, because of the strong coupling between the lattice and the polarization field generated by the longitudinal optical modes in the phonon long-wavelength limit. The polarization field is determined by the dielectric constants and Born effective charges calculated by DFPT in VASP. For LiH (NaH), the Born effective charges of the alkaline metal atom and the hydrogen atom are 1.02 (0.97) e and −1.02 (−0.97) e, respectively, which indicates a strong polarization field, and consequently leads to a large LO/TO splitting of about 92.6 (74.5) rad/ps, as is shown in Fig. 1. For comparison, the result of phonon dispersion for LiH is consistent with that in Ref. [44], but with higher vibration frequencies than those of LiD [44,45]. Similarly, the phonon properties of NaH are also in accordance with the previous results [46,47].

The calculated intrinsic κ_L of LiH and NaH with naturally occurring isotope concentrations as a function of T is plotted in Fig. 2. For LiH, since the fusing point is about 961 K [48–50], we only show the values of κ_L below 950 K in Fig. 2. For NaH, the decomposition temperature is about 700 K at ambient pressure [51,52], and may exceed 1000 K at high hydrogen partial pressure such as 35 MPa calculated by the Clausius-Clapeyron relation $lg\,P_{cm.} = -a/T + b$ with $a = 5070$ and $b = 9.49$ for pure sample [52]. Considering that the pressure of 35 MPa has almost no effect on lattice constant (< 0.05%), we neglect the influence of this pressure on thermal transport, and show the κ_L below 1000 K for NaH in Fig. 2. The iterative solutions (ITS) of the BTE and RTA results are both shown, which reveals a difference of less than 10% between them for $T \geqslant 500$ K. Strikingly, the values of κ_L for these light materials are comparatively low, especially at high temperature. For instance, κ_L of naturally occurring NaH from the ITS (RTA) results is only 3.95 (3.65) W m^{-1} K^{-1} at 900 K, which is similar to that of CdO [11] and $IrSb_3$ [29] at the same temperature, and approximates three to four times of the values for the representative TE materials such as PbTe and PbSe [53,54]. In addition, κ_L of LiH is about 50% to 80% higher than that of NaH as the temperature changing from 300 to 900 K. This result is much inconsistent with the mass difference of about three times between NaH and LiH, suggesting that the mass difference can not fully explain the difference of κ_L. At 300 K, κ_L of LiH is 22.88 (21.80) W m^{-1} K^{-1} from the ITS (RTA) results, which is about 56% larger than the experimental value of 14.70 W m^{-1} K^{-1} [55], but consistent with the previous calculation results [44,56], as shown in Fig. 1 in Ref. [56] and Fig. 7 in Ref. [44].

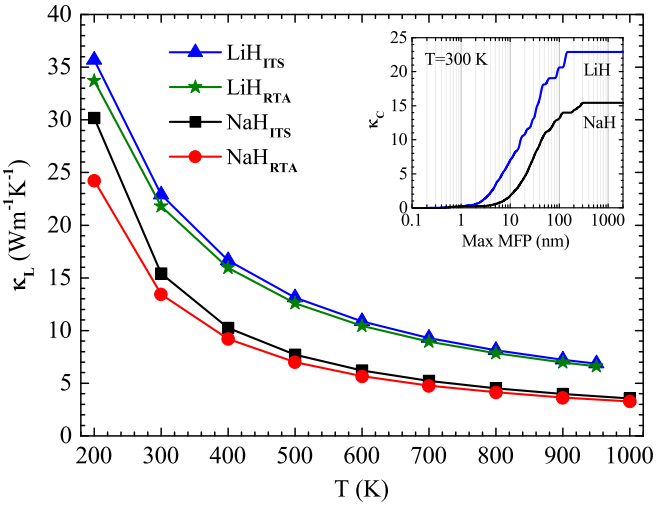

FIG. 2. Lattice thermal conductivity κ_L as a function of T for naturally occurring LiH and NaH. The triangle (pentagram) and square (circle) lines represent the ITS (RTA) results for LiH and NaH, respectively. Inset shows the ITS result of cumulative thermal conductivity κ_C as a function of phonon maximum mean-free path (MFP) for LiH and NaH at 300 K.

Furthermore, we also note that the isotopic effect has almost no influence in determining κ_L of NaH for $T > 200$ K, while the isotopic mass variance plays a significant role in κ_L of LiH at the temperature below 600 K (see S1 in Ref. [57] for κ_L of LiH excluding isotopic effect). Therefore κ_L of LiH will decrease sharply if Li and H atoms are replaced by their heavier isotopes such as ^{7}Li and D. For instance, ^{7}LiD possesses a κ_L of 12.82 W m^{-1} K^{-1} at 300 K [44], which is about a half of the value for the naturally occurring case. For more details, see Ref. [44].

To reveal the detailed thermal transport mechanism, we firstly show the total relaxation times of all phonon modes as functions of frequency in Fig. 3. The total relaxation times are similar for LiH and NaH, with the relaxation times of

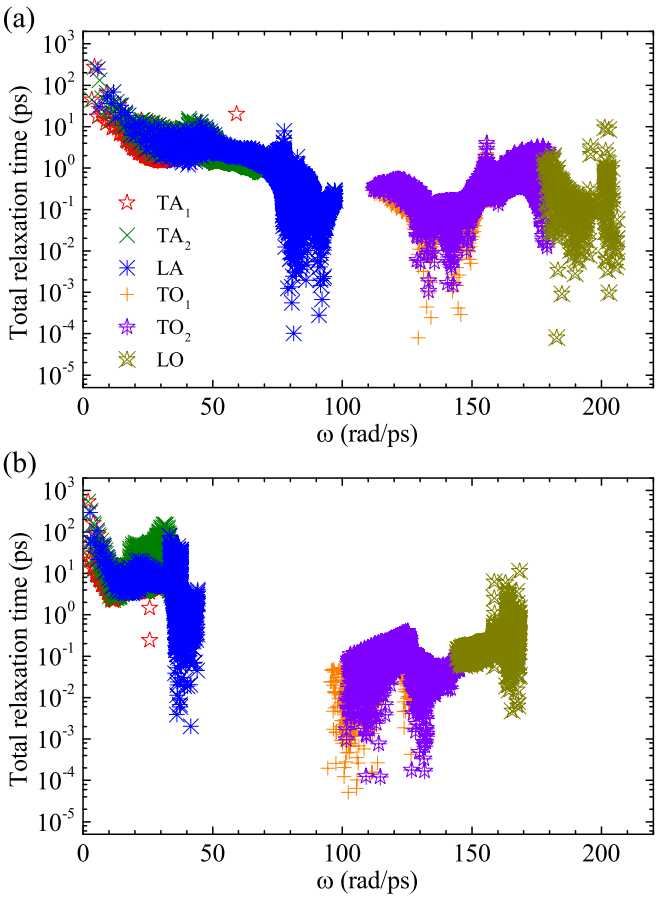

FIG. 3. Total relaxation times of all phonon modes as functions of frequency for LiH (a) and NaH (b) at 300 K.

the optical modes much shorter than those of the acoustic modes. This signifies that the acoustic modes are responsible for most of κ_L. Remarkably, compared with the previous TE materials, the relaxation times for the acoustic modes of LiH and NaH are fairly short, and even shorter than those of PbTe and PbSe [53], which hints a very strong phonon scattering in these light materials. In addition, precise comparison shows that for most of the TA, LA, and LO modes, the relaxation time of LiH is shorter than that of NaH, while for the TO modes, LiH possesses a longer relaxation time. In SHENGBTE calculations, due to the exclusion of boundary scattering effect, the total relaxation time in RTA is obtained by anharmonic three-phonon scattering and isotopic scattering through the relation of $1/\tau_\lambda = 1/\tau_\lambda^{\mathrm{anh}} + 1/\tau_\lambda^{\mathrm{iso}}$. $1/\tau_\lambda^{\mathrm{anh}}$ can be obtained by the sum of the three-phonon transition probabilities $\Gamma^{\pm}_{\lambda\lambda'\lambda''}$, which is determined by the anharmonic IFC3 and the weighted phase space W (a direct measure of the number of scattering processes) [12,58]. Our results show that compared with NaH, LiH possesses a stronger three-phonon scattering (see S2 in Ref. [57]), while it has a smaller weighted phase space W (see S3 in Ref. [57]). The smaller W corresponds to less three-phonon scattering channels, which seems to be contradictory with the stronger anharmonicity of LiH. To explain this, we calculate the κ_L of a hypothetical LiH (NaH), whose IFC3 is replaced by that of NaH (LiH), while all the other quantities remain the same. The result is 55.33 (4.77) $\mathrm{W\,m^{-1}\,K^{-1}}$ for the hypothetical LiH (NaH) at 300 K, in sharp contrast to 22.88 (15.41) $\mathrm{W\,m^{-1}\,K^{-1}}$ for the genuine one at the same temperature. This means that the IFC3 of LiH is much stronger than that of NaH, which is the main reason for the difference of anharmonicity between LiH and NaH. In addition, the isotopic scattering in LiH is also stronger than that in NaH (see S4 in Ref. [57]), which explains the importance of isotopic effect in calculations of κ_L for LiH. The finding is consistent with a stronger isotopic effect of Li atom which, with respect to Na atom, have the features of lighter atomic mass, more stable isotopes, and considerable abundance of each isotope. However, it is worth noting that the strong anharmonic three-phonon scattering is the main reason for the lower κ_L in these light materials, even in LiH at lower temperature. For example, the calculated κ_L of LiH with only anharmonic scattering is 30.95 $\mathrm{W\,m^{-1}\,K^{-1}}$ at 300 K, indicating that the anharmonic scattering takes up about 74% of the total scattering at this temperature. Finally, one can conclude that LiH possesses a relatively short total relaxation time compared to NaH.

The higher κ_L of LiH seems to be contradictory with the shorter total relaxation time in it. To further study the difference of κ_L between LiH and NaH, we show the phonon group velocities within the whole first Brillouin zone in Fig. 4. The phonon group velocities for the nth branch are determined by $v_g = d\omega_n/dq$. With heavier atomic mass, NaH has much smaller group velocities than LiH, especially the group velocities for the acoustic branches. For the TA and LA modes, the maximum group velocities of LiH are about 7.96 and 11.41 km/s, respectively, while those of NaH are about 3.85 and 6.09 km/s, respectively. For the optical modes, LiH and NaH have almost the same group velocities with the maximum values of about 6.50 km/s for the TO modes and 5.50 km/s for the LO modes. In view of $\kappa_L \sim v_g^2$ in RTA, these findings support there exists a higher κ_L in LiH, as is shown

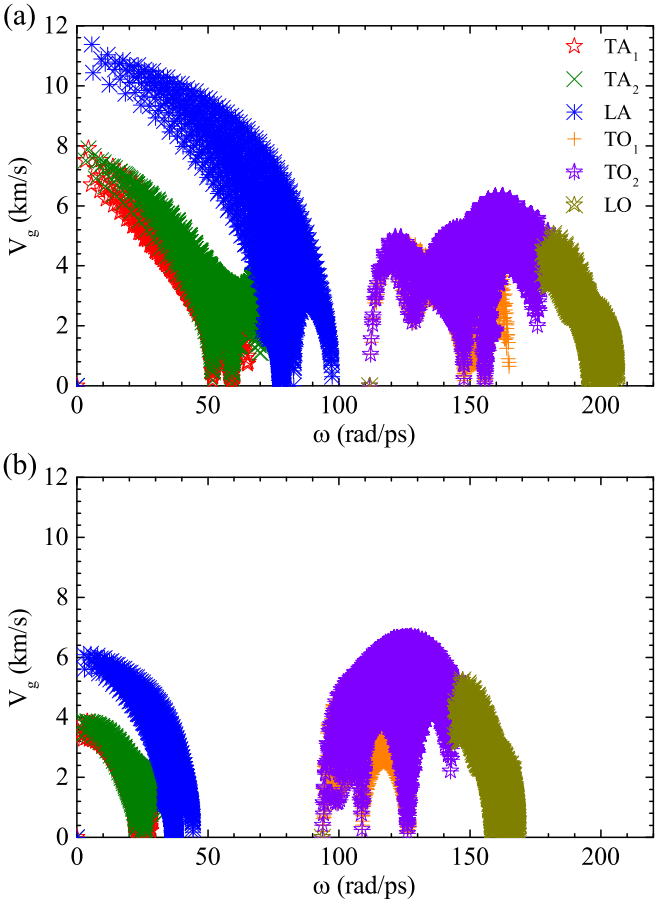

FIG. 4. Phonon group velocities of all phonon modes within the first Brillouin zone as a function of frequency for LiH (a) and NaH (b).

in Fig. 2. Noticeably, the maximum group velocities of NaH are about twice of those of PbTe and PbSe [53]. This is the primary factor that results in κ_L of NaH being higher than those of PbTe and PbSe. Furthermore, from the group velocities combined with the relaxation time, we can also analyze the polarization dependent κ_L. We find that for NaH the optical modes have almost no contribution to κ_L, while for LiH the TO_2 modes contribute about 9% of the total κ_L due to their longer relaxation time (see S5 in Ref. [57] for the polarization dependent κ_L).

In addition, we have also calculated the cumulative thermal conductivity κ_C with respect to the allowed phonon maximum mean-free path (MFP) to study the size dependence of κ_L. κ_C of LiH and NaH at 300 K are plotted in the inset of Fig. 2. The total accumulation keeps increasing as MFPs increases, until reaching the plateau after MFPs increase to 140 nm and 290 nm for LiH and NaH, respectively. The maximum MFPs in LiH and NaH are much longer that those in PbSe and PbTe [53], which is consistent with the high group velocities of these light materials. Furthermore, phonons with MFPs shorter than 100 nm contribute about 80% of the total κ_L for LiH and around 84% for NaH. This means that the nanostructuring with the length of 100 nm would reduce κ_L by 20% for LiH and 16% for NaH. Thus, to significantly reduce κ_L of these materials, nanostructures with the characteristic length shorter than 100 nm are required.

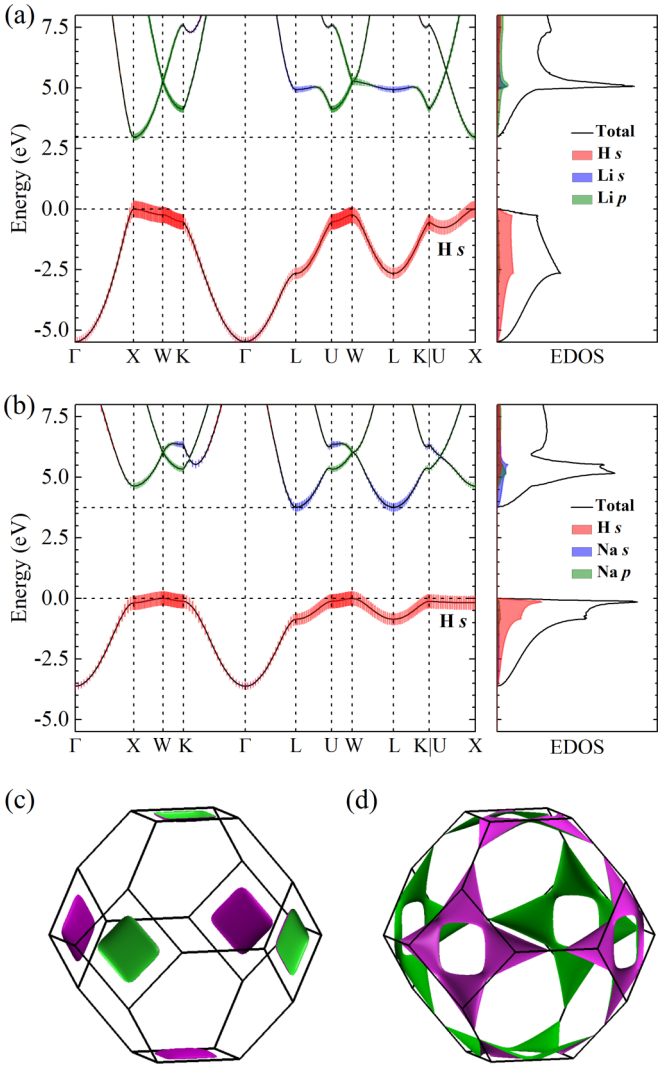

FIG. 5. Projected band structure and EDOS of LiH (a) and NaH (b). The isoenergy surface of LiH (c) and NaH (d) for E_F taken 100 meV into the valence band.

The low κ_L of LiH and NaH would make them be promising TE candidates if their thermopower S and electronic transport properties are good enough. Owing to electronic transport properties are determined by the electronic structures, we show the projected band structure and partial EDOS for LiH and NaH in Figs. 5(a) and 5(b), respectively. We find that LiH has a direct band gap of about 2.96 eV, with the conduction band minimum (CBM) and valence band maximum (VBM) at the X point, while NaH possesses an indirect gap of about 3.75 eV, with the CBM at the L point and the VBM at the W point. These results are in accordance with the previous work which gives the GGA band gaps of 3.00 and 3.79 eV for LiH and NaH, respectively [59]. It is worth noting that the GGA band gap of LiH is about 1.75 and 2.00 eV lower than the GW result and experimental value, respectively [59,60]. Similarly, the GGA gap of NaH is about 2.10 eV lower than the GW result [59]. Partial EDOS together with the projections on band structure show that the valence band is mainly contributed by the hydrogen atoms, while most of the conduction band arises from the alkaline atoms. Moreover, the CBM of LiH is formed from the p orbitals of the alkaline atoms, in contrast with the s orbitals of the alkaline atoms composing the CBM of NaH. Prominently, the band gaps of 2.96 and 3.75 eV for LiH and NaH are much larger than the gaps of most of the known TE materials. Usually, the large band gaps guarantee the high specific heats of carriers, which is a part of reasons why the best TE candidates are mostly semiconductors [1]. We also note that there is a comparatively small dispersion in the valence band, which makes the band around the VBM be fairly flat. Correspondingly, the total EDOS increases very rapidly just below the VBM, especially for NaH. For instance, the EDOS reaches nearly 1.8 states/(eV cell) only at 150 meV below the VBM in NaH. This behavior of valence band implies that there is a large effective mass of electron in LiH and NaH. As is well known, at the constant carrier concentration, the thermopower S is proportional to the effective mass. Thus, high thermopower S is expected in LiH and NaH. In addition, to further understand the behavior of band just below the VBM, we also check the isoenergy (Fermi surface) of the zero temperature LiH and NaH for Fermi level E_F taken a little into the valence band. At 100 meV below the VBM, we find that LiH possesses a two dimensional Fermi sheet centered at the X point, while NaH has a cylinderlike feature along the high-symmetry lines WU and WK in view of the periodicity of the Brillouin zone, see Figs. 5(c) and 5(d). This interprets the quasi step function EDOS in NaH considering that the strictly two-dimensional cylinder has a step function EDOS. Similar feature was also detected at 250 meV below the VBM in PbTe [61]. Compared with PbTe, the cylinderlike feature in NaH is more close to the VBM, which is expected to be beneficial for further improving the TE performance.

To assess the electronic transport and TE properties quantitatively, we use the BOLTZTRAP code to calculate the thermopower S and the electrical conductivity σ/τ as functions of temperature T and doping concentration n for LiH and NaH. All of these calculations are checked by the POSTW90.X program of the WANNIER90 code [62,63], and consistent results are obtained. The calculations with the scissors shift of 2.00 and 2.10 eV for LiH and NaH are also performed, which shows that band gap underestimate have no effect on the thermopower S and electrical conductivity σ/τ. Our results show that the best TE performance is obtained in NaH with the p-type doping, while other cases such as the n-type doped NaH and the p-type doped LiH also show good TE properties. The calculated S and σ/τ as functions of T and n for the p-type doped NaH are plotted in Figs. 6(a) and 6(b), respectively. Being consistent with the electronic Boltzmann theory [38], the σ/τ curve does not depend on T, and increases with the doping concentration n. The thermopower S increases with T at the same n, and decreases with n at the same T, similar to the observed tendency in most of semiconducting TE materials. Strikingly, S is extraordinarily high, as is expected in the band structure analyses. For instance, the values of S for NaH are in the range of 2.22×10^{-4} to 2.85×10^{-4} V K^{-1} as T increases from 500 to 1000 K at $n \sim 1.0 \times 10^{21}$ cm^{-3}, as shown in Fig. 6(a). If the doping concentration lowers, S can be further improved, such as 4.06×10^{-4} V K^{-1} with $n \sim 1.0 \times 10^{20}$ cm^{-3} at $T = 500$ K. These values of S are much higher than that of PbTe, as shown in Fig. 3 in Ref. [2]. Combined with that the typical S for a high-zT material varies

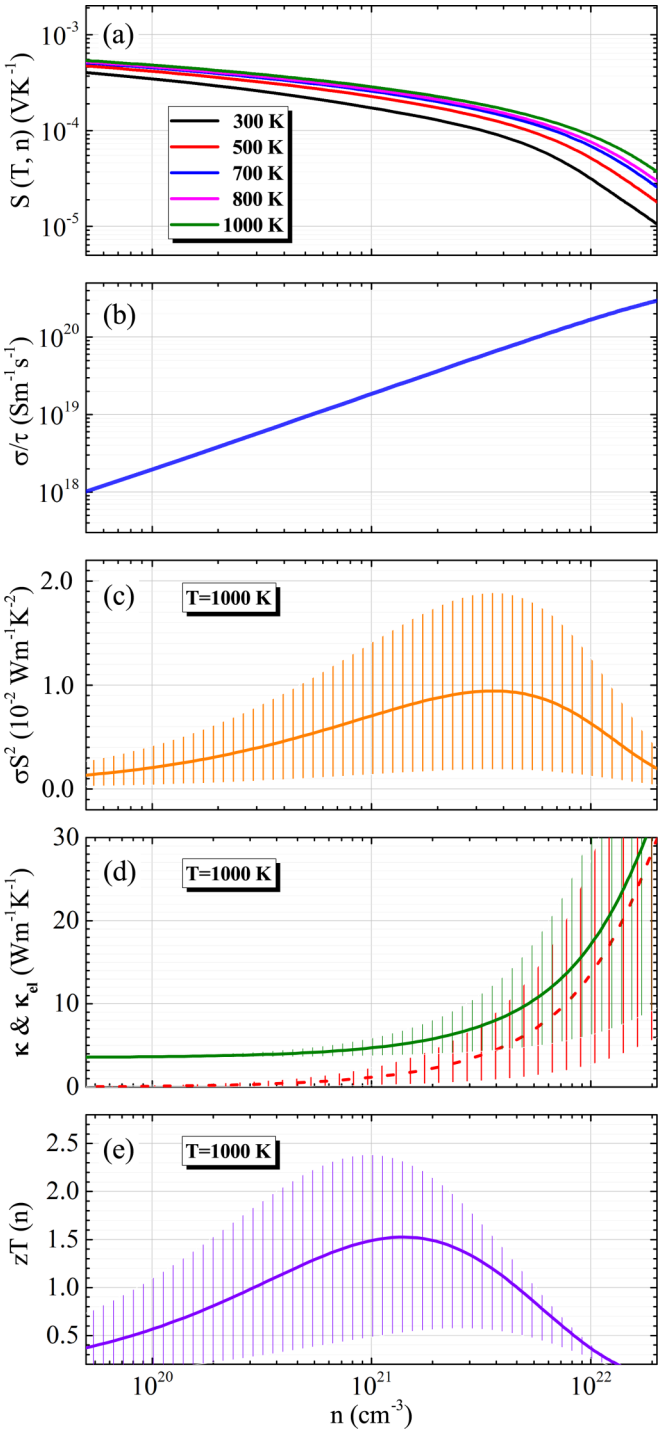

FIG. 6. TE parameters for the p-type doped NaH: (a) Thermopower S at 300 to 1000 K. (b) Electrical conductivity σ/τ. (c) Power factor σS^2. (d) Total thermal conductivity κ (full lines) and electronic thermal conductivity κ_{el} (dash lines). (e) Figure of merit zT. In (c)–(e), the curves and the upper and lower limits of the vertical bars represent the values at 1000 K with $\tau = 5$, 10, and 1 fs, respectively.

between 2.00×10^{-4} and 3.00×10^{-4} V K^{-1}, these results suggest a possible high zT in NaH, although the exact value of σ can not be confirmed at present.

To calculate σ, we firstly use a simple formula $\tau \sim d/v$ to roughly estimate the amplitude of electronic scattering time τ, where d is the average electron-electron distance estimated by the doping concentration, $v = \frac{1}{\hbar}\frac{\partial E(k)}{\partial k}$ is the corresponding electron velocity. From the positive doping concentration $n \sim 10^{21}$ cm^{-3} and the electron velocity $v \sim 10^5$ m/s at this doping level in NaH, τ is found to be about 10 fs. Given the effect of lattice vibration on practical τ, here we use the value of τ from 1 to 10 fs as a substitute in calculations of σ and κ_{el}. In order to obtain a more relevant zT, the electronic thermal conductivity κ_{el} is also included, although it is small compared to κ_L, as shown in Fig. 6(d). Our calculations show that at high temperature zT for the p-type doped NaH often exceeds 1.0 as τ varies between 1 and 10 fs, as shown in Fig. 6(e). With $\tau = 5$ fs, a fairly large $\sigma S^2 \sim 0.79 \times 10^{-2}$ Wm^{-1} K^{-2} and a high $zT \sim 1.53$ are achieved at $T = 1000$ K and $n \sim 1.4 \times 10^{21}$ cm^{-3}, as shown in Figs. 6(c) and 6(e). As τ increases to 10 fs, an extraordinarily high $zT \sim 2.39$ can be reached at $n \sim 1.0 \times 10^{21}$ cm^{-3}, while a maximum zT of 0.60 is obtained at a higher n if τ lowers to only 1 fs, as shown in Fig. 6(e). In addition, for the p-type doped LiH, the maximum zT of 0.88 and 1.35 are obtained at $T = 900$ K with $\tau = 5$ and 10 fs, respectively (see S6 in Ref. [57]). Besides the p-type doping, the cases with n-type doping may also show good TE performance. For example, the maximum zT of 0.82 and 1.28 are achieved in NaH at $T = 1000$ K with $\tau = 5$ and 10 fs, respectively (see S7 in Ref. [57]). By using $zT \geqslant 1.0$ as a criterion, we also check the suitable work temperature for LiH and NaH. With $\tau = 5$ fs, only the p-type doped NaH at $T \geqslant 800$ K meets this criterion. With $\tau = 10$ fs, the temperature leading to $zT \geqslant 1.0$ in the p-type doped NaH decreases into about 650 K, while the p-type doped LiH and n-type doped NaH need $T \geqslant 830$ and 840 K, respectively, to meet this requirement. As an example, see zT of the p-type doped NaH at different temperature in S8 in Ref. [57]. In addition, for the p-type doped NaH, $n \sim 1.0 \times 10^{21}$ cm^{-3} corresponds to about 0.028 holes per primitive cell, which can be realized theoretically by creating a Na vacancy in 36 unit cells. However, due to the tendency toward to decomposition into metal Na and H_2 at high temperature, NaH tends to produce n-type doping. Moreover, for the n-type doping, a much small doping concentration such as $n \sim 1.0 \times 10^{20}$ cm^{-3} (~ 0.003 e/unit cell) is needed to get a zT larger than 1.00, as shown in S7 in Ref. [57], which further lowers the difficulties to realize the n-type doped NaH. A similar tendency also occurs in LiH.

In order to estimate the stabilities of LiH and NaH at high temperature, we also carry out *ab initio* molecular dynamics (MD) calculations. The MD is simulated in a $5 \times 5 \times 5$ invariant supercell containing 250 atoms by the canonical ensemble with a time step of 2 fs. Through 10-ps (5000 steps) MD at 900 K (1000 K) for LiH (NaH), the structure keeps quite intact without any lattice destruction, which suggests a good structural stability. To test the effectiveness of these simulations, we relax the supercell structures generated by MD, and the intact ground-state structures are obtained again, which implies that temperature induced atomic vibrations in our MD simulations have not destroyed the structures. As an example, the bond length evolution of NaH at 1000 K is shown in Fig. S9 in Ref. [57]. From the bond length evolution, we can also find that there is a relatively large bond fluctuation around the balanceable bond lengths in these light materials compared with that in most of heavier materials, which implies

a stronger anharmonicity, and thus complies with the results of the strong anharmonic three-phonon scattering. Notably, at finite temperature, the effect of external pressure is naturally included in these calculations because thermal expansion can not be captured in the MD simulations with invariant supercell, which not only explains the good structural stability of NaH at high temperature but also shows the significant role of external pressure on the stability.

Finally, it is worth to note that it is challengeable to realize TE performance in these light materials at ambient conditions, especially in NaH, because the chemical properties of these materials are fairly active [52,64]. However, at rigid conditions such as water proofing, air proofing, and light shading, TE applications of LiH is probable to be realized. For NaH, to prevent the decomposition at high temperature, the additional conditions such as high purity of sample and external hydrogen partial pressure above 35 MPa are also acquired to realize TE performance [52]. Although these conditions put forward to enormous challenges in design of TE power generator, our calculations support that LiH and NaH are potential TE materials at suitable surroundings.

IV. CONCLUSION

In summary, we have used the Boltzmann transport theory together with first-principles calculations to compute the lattice thermal conductivity κ_L of LiH and NaH. We discover that the calculated κ_L of these light materials are fairly low. Further analyses reveal that the strong anharmonic phonon scattering and the relevant phonon group velocities lead to the low κ_L. A stronger anharmonic phonon scattering is found in LiH, owing to the stronger anharmonic IFC3 of LiH than that of NaH. But a lower κ_L was obtained in NaH because of the much smaller group velocities compared to those in LiH. Then we use a combination of the semiclassical analysis and first-principles calculations to study the thermopower S and electrical conductivity σ/τ of these materials, and conclude that due to the large band gaps and flat band around the Fermi level, S of these materials is extraordinarily high. As a result, a high power factor σS^2 is obtained in LiH and NaH. As the electronic scattering time τ varies between 1 and 10 fs, the figure of merit zT for these materials is often larger than 1.0. Remarkably, a high $zT \sim 1.53$ is achieved in the p-type doped NaH with $\tau = 5$ fs, and a superhigh $zT \sim 2.39$ is obtained in the same NaH with $\tau = 10$ fs. At last, we also carried out a molecular dynamics to confirm the stabilities of LiH and NaH, and found that the pure LiH and NaH are both stable at high temperature. In addition, a relatively large bond fluctuation around the balanceable bond lengths also implies the strong anharmonic three-phonon scattering in these materials. These theoretical results support that crystalline LiH and NaH may be potential materials for thermoelectric applications at suitable conditions such as water proofing, air proofing, light shading, high pressure, and high purity of sample, etc.

ACKNOWLEDGMENTS

This research was supported by the National Key Research and Development Program of China under Grant No. 2016YFB0700102 (Y.Z., S.M., G.L., and J.N.), the National Natural Science Foundation of China under Grants No. 11374175 (Y.Z., S.M., G.L., and J.N.) and No. 11304269 (C.Z.), and the MOST Project of China under Grants No. 2012CB921403 and No. 2015CB921001 (Z.D., C.L., and S.M.).

[1] G. J. Snyder and E. S. Toberer, Nat. Mater. **7**, 105 (2008).
[2] J. P. Heremans, V. Jovovic, E. S. Toberer, A. Saramat, K. Kurosaki, A. Charoenphakdee, S. Yamanaka, and G. J. Snyder, Science **321**, 554 (2008).
[3] J. R. Sootsman, D. Y. Chung, and M. G. Kanatzidis, Angew. Chem. Int. Ed. **48**, 8616 (2009).
[4] M. Zebarjadi, K. Esfarjani, M. S. Dresselhaus, Z. F. Ren, and G. Chen, Energy Environ. Sci. **5**, 5147 (2012).
[5] J. P. Heremans, C. M. Thrush, and D. T. Morelli, Phys. Rev. B **70**, 115334 (2004).
[6] J. Androulakis, I. Todorov, D.-Y. Chung, S. Ballikaya, G. Wang, C. Uher, and M. Kanatzidis, Phys. Rev. B **82**, 115209 (2010).
[7] Y. Pei, X. Shi, A. LaLonde, H. Wang, L. Chen, and G. J. Snyder, Nature (London) **473**, 66 (2011).
[8] J. He, S. N. Girard, M. G. Kanatzidis, and V. P. Dravid, Adv. Funct. Mater. **20**, 764 (2010).
[9] J. He, J. Androulakis, M. G. Kanatzidis, and V. P. Dravid, Nano Lett. **12**, 343 (2011).
[10] M. W. Gaultois and T. D. Sparks, Appl. Phys. Lett. **104**, 113906 (2014).
[11] L. Lindsay and D. S. Parker, Phys. Rev. B **92**, 144301 (2015).
[12] W. Li and N. Mingo, Phys. Rev. B **91**, 144304 (2015).
[13] Q. Hao, D. Xu, N. Lu, and H. Zhao, Phys. Rev. B **93**, 205206 (2016).
[14] Y. Pei, A. LaLonde, S. Iwanaga, and G. J. Snyder, Energy Environ. Sci. **4**, 2085 (2011).
[15] L. D. Hicks and M. S. Dresselhaus, Phys. Rev. B **47**, 12727 (1993).
[16] W. Liu, X. Tan, K. Yin, H. Liu, X. Tang, J. Shi, Q. Zhang, and C. Uher, Phys. Rev. Lett. **108**, 166601 (2012).
[17] M. Zebarjadi, G. Joshi, G. Zhu, B. Yu, A. Minnich, Y. Lan, X. Wang, M. Dresselhaus, Z. Ren, and G. Chen, Nano Lett. **11**, 2225 (2011).
[18] D. Vashaee and A. Shakouri, Phys. Rev. Lett. **92**, 106103 (2004).
[19] J.-H. Bahk, Z. Bian, and A. Shakouri, Phys. Rev. B **87**, 075204 (2013).
[20] Y. Zhang, J.-H. Bahk, J. Lee, C. S. Birkel, M. L. Snedaker, D. Liu, H. Zeng, M. Moskovits, A. Shakouri, and G. D. Stucky, Adv. Mater. **26**, 2755 (2014).
[21] Y. Lan, A. J. Minnich, G. Chen, and Z. Ren, Adv. Funct. Mater. **20**, 357 (2010).
[22] C. J. Vineis, A. Shakouri, A. Majumdar, and M. G. Kanatzidis, Adv. Mater. **22**, 3970 (2010).
[23] K. Biswas, J. He, I. D. Blum, C.-I. Wu, T. P. Hogan, D. N. Seidman, V. P. Dravid, and M. G. Kanatzidis, Nature (London) **489**, 414 (2012).
[24] H. Wang, J.-H. Bahk, C. Kang, J. Hwang, K. Kim, J. Kim, P. Burke, J. E. Bowers, A. C. Gossard, A. Shakouri *et al.*, Proc. Natl. Acad. Sci. USA **111**, 10949 (2014).

[25] L.-D. Zhao, S.-H. Lo, Y. Zhang, H. Sun, G. Tan, C. Uher, C. Wolverton, V. P. Dravid, and M. G. Kanatzidis, Nature (London) **508**, 373 (2014).
[26] S. Sassi, C. Candolfi, J.-B. Vaney, V. Ohorodniichuk, P. Masschelein, A. Dauscher, and B. Lenoir, Appl. Phys. Lett. **104**, 212105 (2014).
[27] C.-L. Chen, H. Wang, Y.-Y. Chen, T. Day, and G. J. Snyder, J. Mater. Chem. A **2**, 11171 (2014).
[28] J. Carrete, N. Mingo, and S. Curtarolo, Appl. Phys. Lett. **105**, 101907 (2014).
[29] W. Li and N. Mingo, Phys. Rev. B **90**, 094302 (2014).
[30] A. Roy, Phys. Rev. B **93**, 100101 (2016).
[31] D. Bayerl and E. Kioupakis, Phys. Rev. B **91**, 165104 (2015).
[32] W. Li, J. Carrete, N. A. Katcho, and N. Mingo, Comput. Phys. Commun. **185**, 1747 (2014).
[33] G. Kresse and J. Furthmüller, Phys. Rev. B **54**, 11169 (1996).
[34] G. Kresse and J. Furthmüller, Comput. Mater. Sci. **6**, 15 (1996).
[35] A. Togo, F. Oba, and I. Tanaka, Phys. Rev. B **78**, 134106 (2008).
[36] G. Kresse and D. Joubert, Phys. Rev. B **59**, 1758 (1999).
[37] J. P. Perdew, K. Burke, and M. Ernzerhof, Phys. Rev. Lett. **77**, 3865 (1996).
[38] G. K. Madsen and D. J. Singh, Comput. Phys. Commun. **175**, 67 (2006).
[39] P. Loubeyre, R. Le Toullec, M. Hanfland, L. Ulivi, F. Datchi, and D. Hausermann, Phys. Rev. B **57**, 10403 (1998).
[40] D. K. Smith and H. Leider, J. Appl. Crystallogr. **1**, 246 (1968).
[41] J. P. Vidal and G. Vidal-Valat, Acta Crystallogr. Sect. B **42**, 131 (1986).
[42] D. R. Stephens and E. M. Lilley, J. Appl. Phys. **39**, 177 (1968).
[43] C. G. Shull, E. O. Wollan, G. A. Morton, and W. L. Davidson, Phys. Rev. **73**, 842 (1948).
[44] L. Lindsay, Phys. Rev. B **94**, 174304 (2016).
[45] J. L. Verble, J. L. Warren, and J. L. Yarnell, Phys. Rev. **168**, 980 (1968).
[46] G. Auffermann, G. D. Barrera, D. Colognesi, G. Corradi, A. J. Ramirez-Cuesta, and M. Zoppi, J. Phys.: Condens. Matter **16**, 5731 (2004).
[47] G. Barrera, D. Colognesi, P. Mitchell, and A. Ramirez-Cuesta, Chem. Phys. **317**, 119 (2005).
[48] C. E. Messer, E. B. Damon, P. C. Maybury, J. Mellor, and R. A. Seales, J. Phys. Chem. **62**, 220 (1958).
[49] F. Pretzel, G. Rupert, C. Mader, E. Storms, G. Gritton, and C. Rushing, J. Phys. Chem. Solids **16**, 10 (1960).
[50] C. E. Messer and J. Mellor, J. Phys. Chem. **64**, 503 (1960).
[51] X. Ke and I. Tanaka, Phys. Rev. B **71**, 024117 (2005).
[52] M. D. Banus, J. J. McSharry, and E. A. Sullivan, J. Am. Chem. Soc. **77**, 2007 (1955).
[53] Z. Tian, J. Garg, K. Esfarjani, T. Shiga, J. Shiomi, and G. Chen, Phys. Rev. B **85**, 184303 (2012).
[54] A. A. El-Sharkawy, A. M. Abou El-Azm, M. I. Kenawy, A. S. Hillal, and H. M. Abu-Basha, Int. J. Thermophys. **4**, 261 (1983).
[55] G. A. Slack, J. Phys. Chem. Solids **34**, 321 (1973).
[56] A. Seko, A. Togo, H. Hayashi, K. Tsuda, L. Chaput, and I. Tanaka, Phys. Rev. Lett. **115**, 205901 (2015).
[57] See Supplemental Material at http://link.aps.org/supplemental/10.1103/PhysRevB.95.014307 for the additional vibrational, thermal, thermoelectric properties of LiH and NaH.
[58] W. Li and N. Mingo, Phys. Rev. B **89**, 184304 (2014).
[59] M. J. van Setten, V. A. Popa, G. A. de Wijs, and G. Brocks, Phys. Rev. B **75**, 035204 (2007).
[60] V. G. Plekhanov, V. A. Pustovarov, A. A. O'Konnel-Bronin, T. A. Betenekova, and S. O. Cholakh, Sov. Phys. Solid State **18**, 2438 (1976).
[61] D. J. Singh, Phys. Rev. B **81**, 195217 (2010).
[62] N. Marzari and D. Vanderbilt, Phys. Rev. B **56**, 12847 (1997).
[63] I. Souza, N. Marzari, and D. Vanderbilt, Phys. Rev. B **65**, 035109 (2001).
[64] J. A. Dilts and E. C. Ashby, Inorg. Chem. **11**, 1230 (1972).